SCALING CRITERIA FOR POOL FIRES DERIVED FROM LARGE SCALE EXPERIMENTS

J. Moorhouse*

Based on experimental studies of the flames from LNG pool fires, scaling criteria are presented for the determination of flame length, flame tilt and flame base dimensions in terms of the pool diameter, fuel burning rate, wind speed and fuel characteristics. These scaling criteria can be used in the determination of the thermal radiation hazard from large fires.

INTRODUCTION

Fires from accidental spillages of liquid fuels from storage tanks or transfer lines can present hazards to personnel, plant and property. The installation of bunding around land based storage tanks is a valuable means of limiting the spread of released liquid and hence limiting the fire hazard. For spills from marine or road tankers, spreading will be less restricted. Pools of liquid can therefore be produced of a variety of shapes and sizes.

In order to be able to determine the potential hazard from such fires it is essential to relate the shape and size of the flame produced to those of the pool and with the local weather conditions, and the nature of the fuel.

Studies have been published covering the nature of flames from large pool fires and it is evident that most hydrocarbon fuels produce luminous flames and generate large quantities of soot. This makes definition of the geometry of the flame somewhat difficult and hence it is common for data to be presented solely in terms of the incident radiation received. It is therefore difficult to make direct comparisons with data for other fuels since values obtained are dependent upon the locations of radiometers with respect to the direction and speed of the wind during the particular experiments.

Fires burning upon pools of liquid natural gas (LNG) are luminous. However, the definition of the visible flame is very distinct since it is not masked by large quantities of soot. Much more precise measurements of the flame geometry can therefore be made and this can be used with a knowledge of flame emissive power to accurately predict thermal

*British Gas Corporation, Research and Development Division, Midlands Research Station, Wharf Lane, Solihull.

radiation levels around the fire. Further, such data is valuable in developing sound theoretical models of the way combustion develops for all types of liquid pool fires.

Flame geometry data for large LNG fires has been published by the American Gas Association (AGA) (1) for spills into 6ft, 20ft and 80ft diameter earthen bunds. In these experiments the pool was ignited shortly after the spill and hence the rate of burning was increased due to heat transfer from the ground adding greatly to the vaporisation of the fuel. The fires were therefore not burning under steady state conditions. The burning of spills of LNG onto water by Raj (2) was also for pools in which the diameter was constantly changing as the liquid spread. Average burning rates were determined from measurements of the average pool diameter and fuel quantity spilled which was then correlated with flame lengths.

In both these studies the flame length was defined as the distance from the centre of the pool to the visible flame tip.

In order to provide data on flame geometry for LNG pool fires burning under both steady conditions and in pools of well defined geometry, a series of experiments have therefore been carried out by the British Gas Corporation, Midlands Research Station.

EXPERIMENTAL TECHNIQUE

The test bund was 12.2m x 15.4m and consisted of a 0.5 metre deep pit with a flat concrete base. The walls of the pit were constructed of engineering blue brick and the top of the walls were flush with local ground level. For each experiment the walls were lined with unfired clay bricks in order to protect the walls from fire damage.

The test bund was provided with slots in the base for locating division blocks, thus ensuring that rectangular pools of different sizes and aspect ratio could be used.

An experiment began by cooling the whole of the base of the selected test section by discharging liquid nitrogen into it. This process generally took at least 30 minutes. When adequately cooled, liquid natural gas was discharged into the bund until a depth of between 10 and 20 cms of liquid had been accumulated. This was achieved in a period of not less than 30 minutes. When adequately cooled, liquid natural gas was discharged into the bund until a depth of between 10 and 20cms of liquid had been accumulated. This was achieved in a period of not less than 30 minutes. This lengthy filling process ensured that the heat transfer from the ground into the liquid was at a low and relatively constant level.

The pool was then ignited to provide a steadily burning pool fire during which the relevant experimental measurements could be made.

Cine film records were made of the fire from two cameras located at right angles to each other. These were arranged so that one was in an upwind position and the other crosswind, although variations in wind direction sometimes occurred so that this ideal was not always achieved.

The depth of the pool of fuel was continuously monitored using a tube dipped into the liquid provided with a slow helium purge which had been previously calibrated for the pressure head in terms of liquid depth.

Continuous measurements of local wind speed and direction were made throughout the test.

A total of 29 experiments were carried out with pool areas varying from 37.2 to 185.8 m^2 in order that the data could be used for extrapolation to other sizes of fires. The tests carried out also covered pools of length to width ratio from 1 to 2.5.

DATA ANAYLSIS

The geometry of the flames was determined by examination of the cine film records.

The flame was found to rapidly achieve a steady burning condition, indicating that an equilibrium was reached between the radiation from the flame and the rate of vaporisation of the fuel. This initial period was ignored in the analysis of the filmed records and measurements were made over a subsequent period of about two minutes.

Three different sets of measurements were made from the films:

1. The area of the flame was determined from flame tracings using a planimeter.

2. Measurements of flame length, flame base diameter and flame tilt were made for which the flame was considered to be represented by a tilted conical shape of base dimension given by the length of the flame base, and length given by the distance between the centre of the flame base and the flame 'tip'.

3. Measurements of flame length, flame base diameter and flame tilt were made for which the flame was considered to be represented by a tilted cylinder of base dimension given by the length of the flame base, and length given by the distance between the centre of the flame base and the flame 'tip'.

Examination of the films revealed that the flame base dimension when viewed from the crosswind position was greater than the pool dimension. This arose due to the extension of the flame base downwind of the pool edge, and is termed flame drag. This phenomenon has been observed elsewhere(3) for laboratory scale experiments. The geometrical shapes of the flame chosen in this study were therefore selected, taking full account of the observed flame base. This represents a significant departure from previous studies of large LNG fires and represents a potential error in the calculation of burning rates for LNG spills onto water since the flame base area is likely to be different from the actual pool area.

In choosing the two idealised flame shapes, i.e. conical and cylindrical, it was recognised, firstly, that neither was a perfect representation since the flame shape changes rapidly with time. Secondly, it was recognised that the shape should not only correspond to the correct viewed area of the flame, but also that the area should be correctly related to the location of that area. For a flame which has been represented as a cylinder of length determined by the visible flame tip, the area at the top of the flame can be considerably over-estimated.

For these reasons, in drawing the two idealised shapes upon photographic images of the flame, a virtual flame tip was chosen such that the area of the flame was equivalent to that of the idealised shape. The reason for measuring actual viewed flame areas using a planimeter was so that comparisons could be made with the two idealised shapes.

Examples of the representations of these idealised shapes superimposed upon an actual flame trace is shown in Figure 1.

For each test between 20 and 30 measurements were made of each of the geometrical parameters and a mean value for each parameter was determined.

Due to variations in wind direction between setting up the cameras and the ignition of the fire the cameras were not always located directly cross wind. In order, therefore, to obtain the true flame length and tilt data from that measured from the two dimensional filmed image of the fire, corrections had to be applied in some cases to the mean measured values.

The following equation was used which is based upon a knowledge of the mean wind direction relative to the line of sight of the camera.

$$\theta = \tan^{-1}\left(\frac{\tan B}{\cos A}\right) \qquad (1)$$

$$L = l\,\frac{\cos B}{\cos \theta} \qquad (2)$$

in which B = mean measured flame tilt
l = mean measured flame length
A = angle between the wind direction and the direction normal to the camera line of sight
θ = true mean flame tilt
L = true mean flame length

The flame drag did not extend over the whole downwind edge of the pool but was most pronounced in the middle. Unfortunately it was not possible to obtain a detailed mapping of the ground level contour of the flame drag and hence the same corrections were not made for the magnitude of the flame drag distance. Instead, flame drag measurements were restricted to those tests where the camera was within 15° of the cross-wind direction and for which any corrections would be small.

EXPERIMENTAL RESULTS

The data obtained from the film analyses for both the cylindrical and conical flame representations is given in Table 1. Also included are the pool dimensions, ambient air density, fuel mass burning rate and mean wind speed.

The data for flame drag is expressed as the flame drag ratio D'/Dw in which D' is the visible flame base length and Dw is the maximum pool dimension in the direction of the wind. This approach is shown diagramatically in Figure 2 and was adopted since it was recognised that for rectangular pools the extent of flame drag could be influenced by the wind direction in relation to the major and minor axes of the bund.

The basic data is shown graphically in Figures 3,4 and 5, for flame tilt as a function of wind speed, flame drag ratio as a function of wind speed,

and dimensionless flame length as a function of pool diameter respectively. The data is shown for both the conical and cylindrical flame representations, and it is evident that it is difficult to draw meaningful trends when presented in this way.

FLAME GEOMETRY CORRELATIONS

In order to transform the data into useable generalised forms, correlations of the relevant parameters were made. These were made using the same form as previously published equations as discussed below.

FLAME LENGTH CORRELATION

The relationship developed by Thomas (4) for calm wind conditons based on data for burning wooden cribs is:

$$\frac{L}{D} = 42\left(\frac{m}{\rho a\sqrt{gD}}\right)^{0.61} \qquad (3)$$

in which m = mass burning rate
ρa = ambient air density
g = gravitational constant
D = base diameter of the fire

Under wind blown conditions (5) this equation was modified to:

$$\frac{L}{D} = 55\left(\frac{m}{\rho a\sqrt{gD}}\right)^{0.67}\left(U^*\right)^{0.21} \qquad (4)$$

in which U* is the dimensionless wind velocity given by:

$$U^* = \frac{U}{Uc}$$

in which U = wind velocity
Uc = characteristic wind velocity

defined as $$Uc = \left(\frac{g\,m\,D}{\rho a}\right)^{\frac{1}{3}} \qquad (5)$$

In equation 4, for values of U less than Uc, U* is assigned the value of unity. For wind velocities up to the characteristic value the flame length therefore remains constant whilst at higher values flame shortening occurs.

An equation of similar form to equation 4 was derived by the AGA (1) from their experimental data:

$$\frac{L}{D} = \left(\frac{m}{\rho a\sqrt{gD}}\right)^{-0.19}\left(U^*\right)^{0.06} \qquad (6)$$

This equation is inconsistent with the Thomas equation in that an increase in mass burning rate, for a given pool size, results in a decrease in flame length, and further that as the wind speed increases so does the flame length.

Since no data was obtained in these experiments of LNG fires under zero wind conditions no attempt was made to develop relationships similar in form to equation 3.

Computer correlations were however made of the data with the three dimensionless groups in equation 4 for both cylindrical and conical flame representations. The equations obtained were:

Conical flame representation:-

$$\frac{L}{De} = 4.7 \left(\frac{m}{\rho a \sqrt{g\, De}} \right)^{0.21} \left(U_{10}^{*} \right)^{-0.114} \qquad (7)$$

Cylindrical flame representation:-

$$\frac{L}{De} = 6.2 \left(\frac{m}{\rho a \sqrt{g\, De}} \right)^{0.254} \left(U_{10}^{*} \right)^{-0.044} \qquad (8)$$

in which U_{10} is the wind speed at 10m above ground level and De is the equivalent circular pool diameter.

Both these equations are valid for U_{10} greater than Uc. For U_{10} less than Uc the dimensionless wind speed term is assumed to be unity. The equations show the tendency for the dimensionless flame length to increase with increasing burning rate and to decrease with increasing wind speed, both these trends being consistent with the Thomas equation. The quality of the fit of the equation to the data is shown in Figure 6 for the case of the conical flame representation. A similar degree of fit has been obtained for the cylindrical flame representation.

Flame Tilt Correlations

There are two types of equations given in the literature for predicting the flame tilt, θ, of wind blown fires.

The relationship developed by Thomas (4) is based on data for burning wooden cribs and is given by:

$$\cos\theta = 0.7 \left(U^{*} \right)^{-0.49} \qquad (9)$$

in which $U^{*} = \frac{U}{Uc}$ and $Uc = \left(\frac{g m D}{\rho a} \right)^{1/3}$

and for values of U less than Uc, U* is taken to be unity and hence no flame tilt occurs until the characteristic velocity is achieved.

An equivalent equation was obtained by the AGA for large LNG fires:

$$\cos\theta = \left(U^{*} \right)^{-0.5} \qquad (10)$$

and in this case UC is given by $\left(\frac{g m D}{\rho v} \right)^{1/3}$

which uses ρv the fuel vapour density rather than the ambient air density as used by Thomas.

On the basis of studies of small pools of various liquid fuels, Welker and Sliepcevich (3) developed the equation:

$$\frac{\tan\theta}{\cos\theta} = 3.3 \left(F_r \right)^{0.8} \left(Re \right)^{0.07} \left(\frac{\rho v}{\rho a} \right)^{-0.6} \qquad (11)$$

in which the Froude and Reynolds numbers are given by:

$$F_r = \frac{U^2}{g D} \quad , \quad Re = \frac{D U}{\gamma}$$

in which γ is the kinematic viscosity of air.

The final term in equation 11 is intended to reflect the differences obtained for the different fueld studied.

The data obtained in these large LNG pool fire experiments have been correlated with the variable terms in equations 9 and 11. This has been done for both the conical and cylindrical flame representations.

Thomas type equation:-

a) Conical flame representation

$$\cos\theta = 0.87 \left(U_{10}^{*} \right)^{-0.272} \qquad (12)$$

b) Cylindrical flame representation

$$\cos\theta = 0.86 \left(U_{10}^{*} \right)^{-0.250} \qquad (13)$$

Welker and Sliepcevich type equation:-

a) Conical flame representation

$$\frac{\tan\theta}{\cos\theta} = 3.0 \left(Fr_{10} \right)^{0.422} \left(Re_{10} \right)^{0.011} \qquad (14)$$

b) Cylindrical flame representation

$$\frac{\tan\theta}{\cos\theta} = 1.9 \left(Fr_{10} \right)^{0.399} \left(Re_{10} \right)^{0.050} \qquad (15)$$

In equations 14 and 15 the density ratio term has been incorporated into the constant since the data is for one fuel only.

The suffix '10' denotes that the Reynolds and Froude numbers are based on wind speeds at 10 metres above ground level.

The quality of the fit of these equations is shown in Figures 7 and 8 for the cylindrical flame representations.

The quality of the fits is good although one data point in Figure 8 shows a significant deviation. In this particular test for a 148.5m pool the flame was of a different character to the other fires having similarities with flames on very much smaller pools, and in this test the wind speed was one of

the lowest recorded in this series.

For fires in much larger pools this type of behaviour would be expected to occur at higher wind speeds as predicted by equations 12 and 13.

Flame Drag Correlations

It is evident from Figure 4 that flame drag has a strong dependence upon wind speed, The flame drag phenomenon was not reported by Thomas for burning wooden cribs, and although photographs of the American Gas Association LNG pool fires clearly show its existence, it is not reported.

A detailed study is however reported by Welker and Sliepcevitch for small circular pool fires in a wind tunnel using different fuels, and the data was represented by the equation

$$\frac{D'}{D}\left(\frac{\rho_v}{\rho_a}\right)^{-0.48} = 2.1\left(F_r\right)^{0.21} \qquad (16)$$

in which D'is the actual elongated flame base dimension and D is the circular pool diameter.

The large scale LNG pool fires reported here are for square and rectangular pools and the extent of flame drag was expressed as D'/Dw for the reasons presented earlier.

Correlation of the data using a similar form to equation 16 gives

a) Conical flame representation

$$\frac{D'}{Dw} = 1.6\left(F_{r_{10}}\right)^{0.061} \qquad (17)$$

b) Cylindrical flame representation

$$\frac{D'}{Dw} = 1.5\left(F_{r_{10}}\right)^{0.069} \qquad (18)$$

These equations give a good fit to the data, as shown in Figure 9 for the conical flame representation.

The flame drag observed is essentially an extension of the base of the flame downwind of the pool, whilst the upwind edge of the flame and the flame width is unchanged. These studies have not allowed a detailed mapping of the ground contour of the flame extension, but in order to use the data it is convenient to assume that the flame base is elliptical in shape with one axis equal to the bund width and the other axis equal to the extended flame base.

Since the tilting of a flame assumed to be cylindrical in shape generates an elliptical base at ground level, albeit that the centre of the base needs to be displaced downwind, it might be expected that the flame drag would be directly related to the angle of tilt. If this was the case then $\frac{D'}{Dw}$ would equal $\frac{1}{\cos\theta}$

This possibility has been investigated as shown in Figure 10 from which it is evident that a correlation does exist, but flame drag ratios are generally less than those given by $\frac{1}{\cos\theta}$

In developing a flame profile for use in thermal radiation calculations the flame tilt and flame drag are therefore best determined independently using the separate equations developed.

It should be recognised that the data obtained for flame drag is for square and rectangular pools with aspect ratios not exceed 2.5:1. Further, in no case was data obtained for wind direction directly along the diagonal of a bund. The tests were also carried out for bunds with the tops of the walls flush with ground level and this may influence the extent of flame drag, as has been observed for small laboratory fires (6).

A similar type of behaviour has however been observed for fires burning on the top of fuel tanks, and the derived equation may find application for such situations.

DISCUSSION AND CONCLUSIONS

A series of equations has been obtained based on steady burning LNG pool fire data which can be used for determining whether the flames are likely to impinge upon adjacent plant or equipment, and as a basis for calculating the thermal radiation incident upon plant or personnel.

In designing to prevent flame impingement it is important to use the equations developed for the conical flame representation since these give the largest flame lengths.

For the calculation of thermal radiation levels it is important that the view factor between flame and target is correctly determined. It is considered that previous representations of flames from LNG pool fires which have defined the flame as a cylinder of height determined by the flame tip can significantly over-estimate the flame area as illustrated in Figure 1 and hence over-estimate the view factors. The geometrical representations adopted in this paper are considered to be more realistic. In order to confirm this, comparisons were made between the area of the flame given by the cylindrical and conical flame representations and the flame area measured using a planimeter. It was found that the two dimensional areas for cylindrical flames agreed well with the measured areas, although in general values for the cylindrical flame were up to 10% too high. For the conical flame the areas were always smaller than the measured values.

It is concluded therefore that for thermal radiation calculations the cylindrical flame representation approach is most appropriate.

Adoption of a cylindrical flame geometry of height determined by the flame tip can therefore cause over-estimates of incident flux levels due to the greater than actual flame areas. Allowance can be made for this by adopting an appropriate value of average flame emissive power. This approach can be used for predicting radiation levels at positions remote from the fire where the actual shape of the flame has no significant influence on the calculated view factors. It can however give under-estimates of radiation levels at positions close to the fire since in these cases it is the view factor derived from the flame area at the base of the flame which is much more important that that at the top.

Calculation of radiation levels should also incorpoate the observed flame drag since this not only increases the flame area at the base, but also brings the surface of the flame closer to some receiving surfaces.

The preferred flame geometry for use in calculating thermal radiation levels around LNG fires therefore consists of a flame of elliptical cross-section in a horizontal plane, which maintains this cross section with height, the axes of the ellipse being determined by the bund dimensions and the wind speed. This approach can be applied for pools of aspect ratio similar to those studied. It is unfortunately not possible to apply the equation to fires in long slots, and this topic warrants further investigation.

It is evident from the above discussion that the position from which a flame is viewed will determine the shape that the flame appears to adopt. Measurements of thermal radiation levels from fires must therefore be made with this in mind and care must be taken in translating these values into a thermal emissive power for the surface of the flame.

REFERENCES

1. American Gas Association, November 1973. LNG Safety Program Phase II - Consequences of LNG Spills on Land. Project 1S-3-1.

2. Raj P.P.K., Moussa A.N., and Aravamudan K., 1979, "Experiements Involving Pool and Vapour Fires from Spills of Liquefied Natural Gas on Water", Report No. CG-D-55-79, U.S. Department of Transportation.

3. Welker J.R. and Sliepcevich C.M. 1966. Fire Technology 2.

4. Thomas P.H. 1963, 9th Symposium (International) on Combustion, 844.

5. Thomas P.H. 1965, Fire Research Note No. 600, Fire Research Station, Borehamwood, England.

6. Burgess D.S., Strasser A., and Grumer J., 1961. Fire Research Abstracts and Reviews 3 3, 177.

SYMBOLS USED

A	=	angle between the wind direction and the direction normal to the camera line of sight. (degree).
B	=	mean measured flame tilt (degree)
D'	=	pool diameter (m)
D	=	elongated flame base dimension (m).
Dw	=	maximum pool dimension in the direction of the wind (m).
De	=	equivalent circular pool diameter (m).
Fr	=	Froude number
g	=	gravitational constant (m/s^2)
ℓ	=	mean measured flame length (m)
L	=	true mean flame length (m)
m	=	mass burning rate (Kg/m^2s)
Re	=	Reynolds number
U	=	Wind velocity (m/s)
U*	=	dimensionless wind velocity
U_{10}	=	wind velocity at 10m above ground level (m/s)
U_{10}*	=	dimensionless wind velocity using U_{10} (m/s)
Uc	=	characteristic wind velocity (m/s)
θ	=	true mean flame tilt (degree)
γ	=	kinematic viscosity of air (m^2/s)
ρa	=	air density (kg/m^3)
ρv	=	density of fuel vapour at normal boiling point (kg/m^3)

ACKNOWLEDGEMENTS

The author would like to acknowledge the contributions made to the work described in this paper by numerous colleagues within British Gas, and in particular to Mr. S. Hammond.

This paper is published by permission of British Gas.

Table 1 - Flame Geometry Data obtained from LNG Pool Fire experiments

Pool Length (m)	Pool Width (m)	Equivalent Circular pool Diameter Dc (m)	Ambient air Density (kg/m³)	Fuel mass Burning rate m (kg/m² s)	Wind Speed U 10m (m/s)	Conical Flame Representation: Flame Length L (m)	Flame Tilt θ (degrees)	Downwind Flame base D¹ (m)	Flame drag Ratio (D¹/Dw)	Cylindrical Flame Representation: Flame Length L (m)	Flame Tilt θ (degrees)	Downwind flame base D¹ (m)	Flame Drag Ratio (D¹/Dw)
6.10	6.10	6.88	1.211	0.089	3.9	22.1	50.9	-	-	9.3	50.3	-	-
6.10	6.10	6.88	1.225	0.166	8.0	15.7	47.7	-	-	7.9	49.3	-	-
6.10	6.10	6.88	1.262	0.100	3.0	18.1	30.6	-	-	16.5	28.5	-	-
6.10	6.10	6.88	1.233	0.110	3.3	18.9	29.8	25.0	1.25	14.1	34.0	21.6	1.08
6.10	6.10	6.88	1.245	0.076	1.8	16.0	40.3	25.2	1.26	11.1	45.0	25.0	1.25
6.10	6.10	6.88	1.257	0.099	8.7	14.6	50.7	27.8	1.39	13.5	46.0	28.2	1.41
6.10	6.10	6.88	1.204	0.078	10.0	13.0	59.4	28.8	1.44	12.5	62.7	29.6	1.48
6.10	6.10	6.88	1.220	0.107	4.5	16.9	46.2	25.8	1.29	15.3	48.5	30.4	1.52
6.10	6.10	6.88	1.240	0.096	13.6	13.5	68.8	-	-	11.3	70.0	-	-
9.14	6.10	8.42	1.212	0.053	2.7	13.1	40.0	-	-	9.4	35.1	-	-
9.14	6.10	8.42	1.179	-	2.1	22.6	33.6	-	-	20.4	39.2	-	-
12.19	6.10	9.73	1.217	0.094	12.4	21.0	64.5	-	-	12.8	48.9	-	-
12.19	6.10	9.73	1.190	0.128	5.1	17.2	49.4	53.6	1.34	15.0	46.0	51.6	1.29
15.24	6.10	10.88	1.165	0.136	2.7	24.1	42.1	-	-	21.0	43.6	-	-
15.24	6.10	10.88	1.66	0.133	4.5	28.4	49.9	-	-	16.7	38.9	-	-
12.19	9.14	11.91	1.176	0.108	10.6	20.3	53.6	-	-	19.0	66.4	-	-
15.24	6.10	10.88	1.153	0.045	6.0	26.1	48.8	-	-	14.8	47.7	-	-
6.10	6.10	6.88	1.206	0.056	13.5	12.9	62.7	-	-	11.1	62.9	-	-
12.19	9.14	11.91	1.167	0.079	9.3	26.7	44.0	-	-	20.0	47.0	-	-
12.19	12.19	13.76	1.246	0.100	7.8	26.5	59.3	59.6	1.49	22.8	63.4	62.0	1.55
12.19	12.19	13.76	1.160	-	8.7	31.4	53.0	59.2	1.48	25.2	54.7	61.2	1.53
12.19	12.19	13.76	1.169	-	2.2	27.2	11.1	56.6	1.00	23.4	15.2	51.5	0.91
12.19	12.19	13.76	1.213	0.094	12.0	29.4	60.2	61.2	1.53	21.3	57.0	60.0	1.50
12.19	12.19	13.76	1.225	0.149	13.5	34.4	57.9	77.5	1.37	26.9	58.0	78.6	1.39
15.24	12.19	15.38	1.224	0.110	7.2	23.7	53.5	-	-	25.2	57.1	-	-
15.24	12.19	15.38	1.196	0.119	14.4	29.8	60.1	-	-	23.4	59.0	-	-
15.24	6.10	10.88	1.2[illegible]	0.086	6.7	17.8	56.3	40.8	1.44	12.0	52.5	38.3	1.35
15.24	12.19	15.38	1.190	-	3.9	29.6	54.4	67.0	1.34	29.2	56.8	69.0	1.38
15.24	12.19	15.38	1.185	0.108	7.9	29.5	58.5	-	-	26.1	56.5	-	-

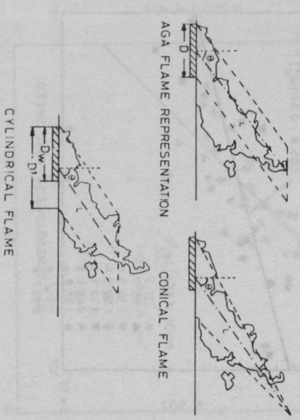

Figure 1 Geometrical representations of an LNG fire

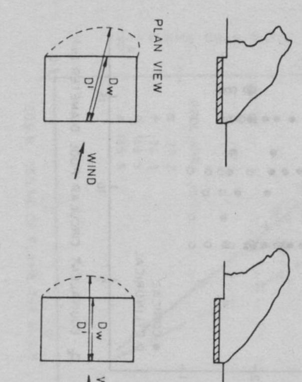

Figure 2 Method of representation of flame drag

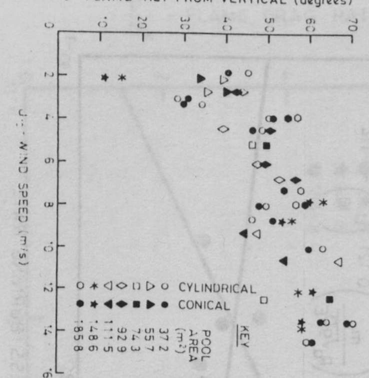

Figure 3 Dependence of flame tilt on wind speed

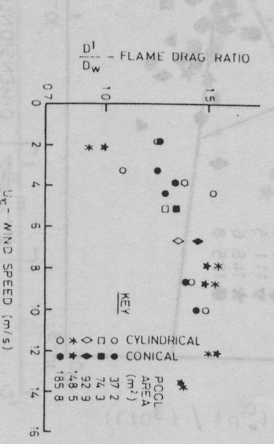

Figure 4 Dependence of flame drag ratio on wind speed

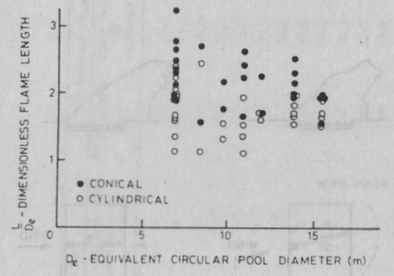

Figure 5 Dependence of flame length on pool diameter

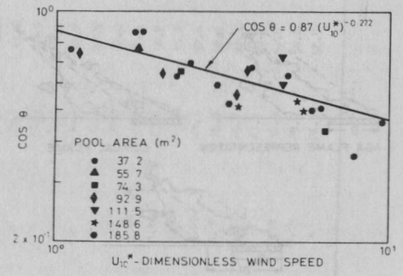

Figure 7 Comparison of derived tilt equation with data (Conical representation)

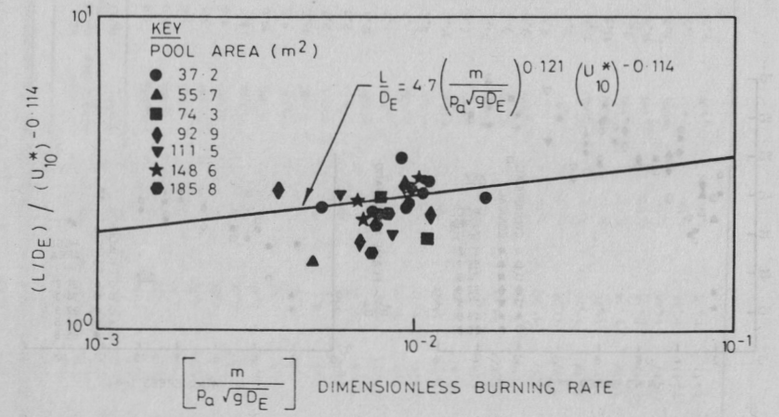

Figure 6 Comparison of derived flame length correlation with experimental data (Conical flame representation)

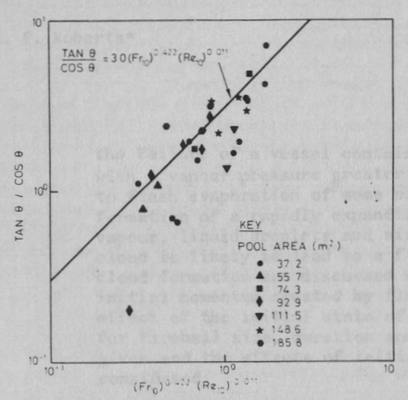

Figure 8 Comparison of derived tilt equation with data(Conical representation)

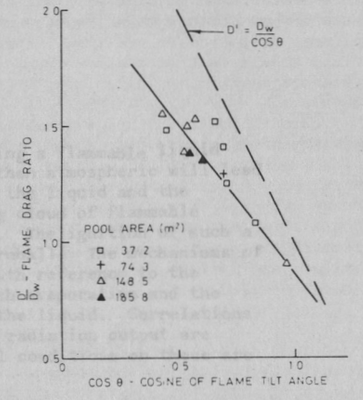

Figure 10 Relationship between flame drag ratio and cosine of tilt angle

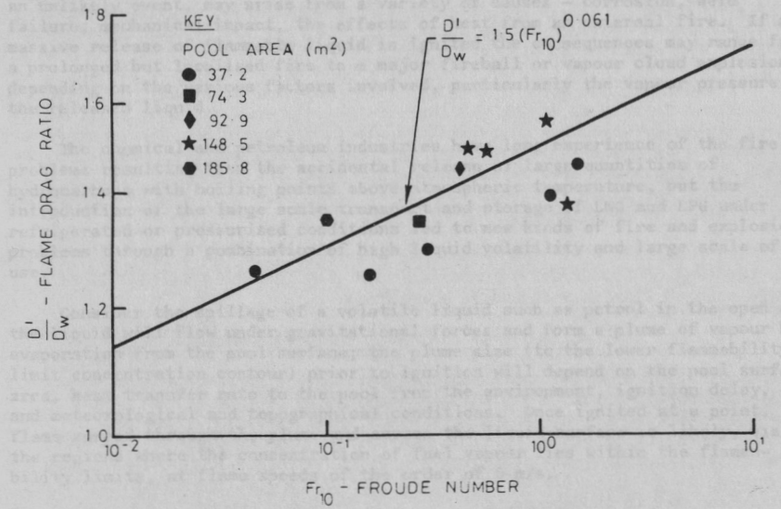

Figure 9 Comparison of derived flame drag correlation with data (Conical flame representation)